

Flexible, durable and magnetic nanofibrous membrane with pH-switchable wettability for efficient on-demand oil/water separation

Wenjing Ma¹, Mengjie Zhang², Yuansheng Li², Mengmeng Kang¹, Chaobo Huang^{2, *},
Guodong Fu^{1, *}

1. College of Chemistry and Chemical Engineering, Southeast University (SEU), Nanjing, 211189, P. R. China
2. College of Chemical Engineering, Jiangsu Provincial Key Lab for the Chemistry and Utilization of Agro-forest Biomass, Jiangsu Key Lab of Biomass-based Green Fuels and Chemicals, Nanjing Forestry University (NFU), Nanjing, 210037, P. R. China

Corresponding authors

Tel: +86-25-85427532; Fax: +86-25-85427532; Email: Chaobo.Huang@njfu.edu.cn
(Chaobo Huang);

Tel.: +86-25-52090625; Fax: +86-25-52090625; Email: 101010855@seu.edu.cn
(Guodong Fu)

1. Experiment

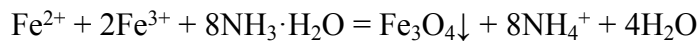
1.1. Preparation of Polyimide (PAA)

The PAA was prepared according to our previous report [1]. Briefly, equal molar ratios of BPDA and PDA were reacted in DMAc at $-5\text{ }^{\circ}\text{C}$ for 24 h. Then the obtained light yellow viscous PAA solution containing 7.1 wt % PAA was re-dissolved in DMAc to prepare a spinning solution (3 wt% PAA). Meanwhile, 1 wt % CTAB was added to enhance the conductivity of electrospinning solution.

1.2. Synthesis of Fe_3O_4 nanoparticles

The magnetite Fe_3O_4 nanoparticles were prepared by the chemical co-precipitation

method[2]. Typically, 2.01 g of $\text{FeCl}_2 \cdot 4\text{H}_2\text{O}$ and 4.81 g of $\text{FeCl}_3 \cdot 6\text{H}_2\text{O}$, with the molar ratio of ferric ion to ferrous ion in the solution of 3.53, were dissolved in 120 mL of oxygen-free distilled water and stirred for 30 min to obtain a homogeneous solution. Subsequently, 10 mL of $\text{NH}_3 \cdot \text{H}_2\text{O}$ (28%) was added into the iron salt solution, and meanwhile, purged with pure nitrogen. In the following, the system under vigorous stirring at 70 °C for 30 min. The solution color changed from orange to black, this is the required condition for precipitation of the containing particles. Possible reaction for the formation of Fe_3O_4 particles was presented as below:



The precipitation was then magnetically separated and collected using a magnet, then the gathered precipitation was re-dispersed into deionized water and ethanol for 5 times to remove the excess amine molecules. Finally, the obtained fine Fe_3O_4 nanoparticles were dried at room temperature under vacuum for 24 h.

1.3. Preparation of PI nanofibrous membrane

Electrospinning was carried out on electrospinning machine (FM1206, Beijing Future Material Sci-tech, China). The PAA solution was spun from a syringe equipped with a 21-gauge needle at a constant delivery rate of $1.0 \text{ mL} \cdot \text{h}^{-1}$. A flywheel rotated at 1500 rpm to collect nanofibers. The distance between the needle tip to the collector was 10 cm, and the applied voltage was set as 15-20 kV. Then, the electrospun nanofiber membranes were thermally imidization using the following protocol under nitrogen atmosphere: heating up to 150, 200, 250, 300, 350, and 380 °C at a rate of $1 \text{ }^\circ\text{C min}^{-1}$, and staying at each temperature stage for 1, 1, 1, 1, 3 and 0.5 h, respectively.

1.4. Preparation of $\text{Fe}_3\text{O}_4/\text{MA-TiO}_2$ coating solution

First, 2 g of Myristic acid were completely dissolved in 150 mL of ethanol under ultra-sonication. Then, dropwise addition of 2.52 mL of $\text{Ti}(\text{O}i\text{Bu})_4$ under stirring at ambient temperature. After stirred vigorously for another 10 min, 100 μL of a 0.1 M

HCl aqueous solution and 2 mL of deionized water were added into the above mixture while stirring vigorous for 30 min at room temperature to obtain a white TiO₂ sol, which was marked as MA-TiO₂ solution. Finally, to this white sol, 3 mL of iron oxide nanoparticles (1 wt%, dispersed in ethanol) was introduced and dispersed ultrasonically for 60 min to form Fe₃O₄/MA-TiO₂ coating solution.

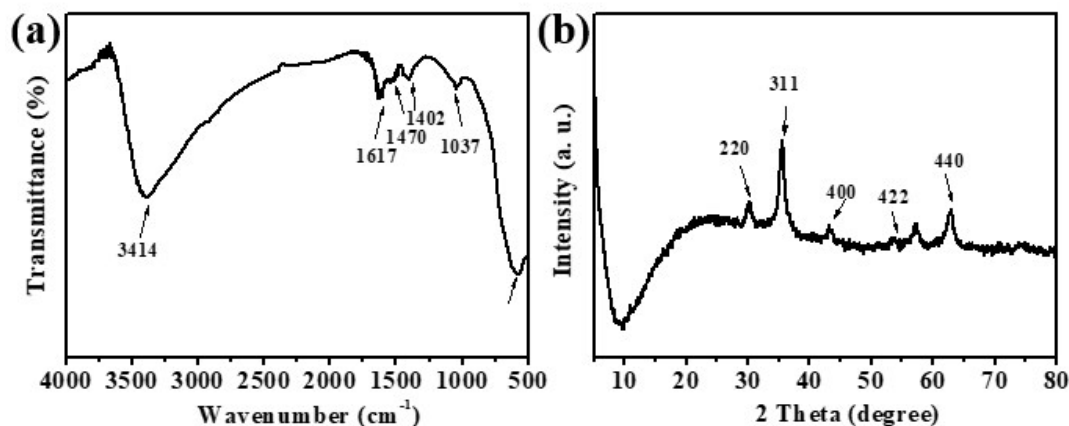


Figure S1 (a) FT-IR and XRD (b) spectrum of Fe₃O₄ nanoparticles

In the FTIR spectrum of Fe₃O₄ nanoparticles, the absorption peaks at 3414 cm⁻¹ could be assigned to the O-H stretching [3], whereas those at 1402 and 1470 cm⁻¹ represented H-O-H bonding vibration of water[4]. The characteristic peaks at 1617 and 1037 cm⁻¹ corresponded to the absorption peaks of $\nu_{\text{O-H}}$ and $\delta_{\text{O-H}}$ [5]. Fig. S1 (b) shows the XRD patterns for Fe₃O₄ nanoparticles. Six characteristic peaks ($2\theta = 30.1, 35.5, 43.1, 53.4, 57.0, \text{ and } 62.6^\circ$) were observed in the XRD pattern of Fe₃O₄ nanoparticles, marking their indices ((220), (311), (400), (422), (511), and (440)), in accordance with those reported in previous literature [6].

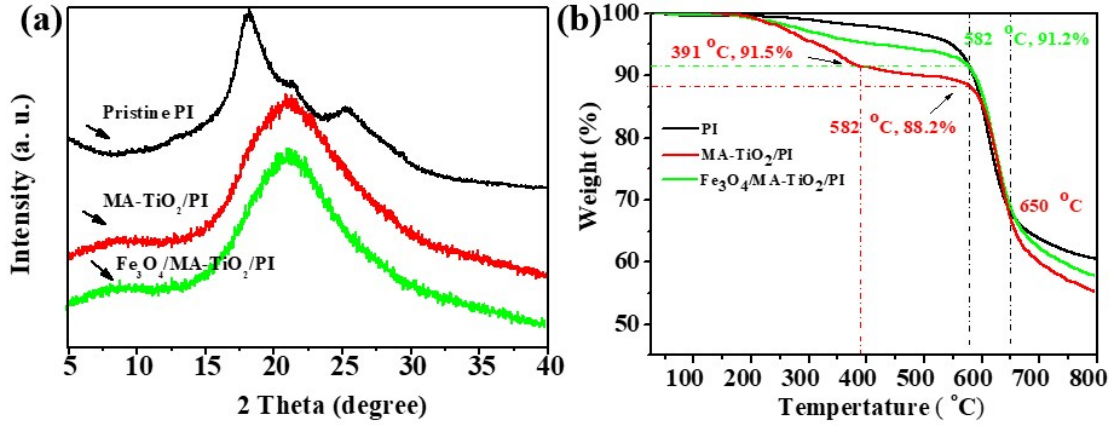


Figure S2. (a) TGA curves, and (b) XRD patterns of pristine PI, MA-TiO₂/PI membrane and Fe₃O₄/MA-TiO₂/PI membrane.

Additionally, the composition of the as-prepared membrane was further analyzed from TGA curves due to different thermal stability of pristine PI nanofibrous membrane, MA-TiO₂ and Fe₃O₄ nanoparticles. As shown in Fig. S2a, the original PI membrane under the weight loss in two steps. The first stage was from room temperature to 540 °C with a negligible weight loss, which can be attribute to the loss of adsorbed water. The second stage was from 540 to 660 °C with an obvious mass loss of 33.3%, which was mainly due to the decomposition of PI. Unlike PI membrane, the weight loss of the MA-TiO₂/PI membrane starts at 100 °C and decreased about 9.5% of its mass when the temperature raised to 540 °C. Compared with PI and MA-TiO₂/PI membranes, the weight loss about 13.5% of Fe₃O₄/MA-TiO₂/PI membrane from 200 to 540 °C is related to MA-TiO₂ and Fe₃O₄. In addition, it was worth mention that all the membranes were not entire weight loss at 800 °C due to their incomplete decomposition. These results demonstrated that the Fe₃O₄/MA-TiO₂/PI membrane was prepared successfully.

Meanwhile, the fiber patterns of the membranes were also investigated. As displayed in Fig. S2b, the diffraction patterns of pristine membrane and the coated membrane did not show a significant different, indicating the successful deposition of Fe₃O₄ and MA-TiO₂ sol on the PI nanofibrous membrane and the fiber pattern was preserved during the surface treatments.

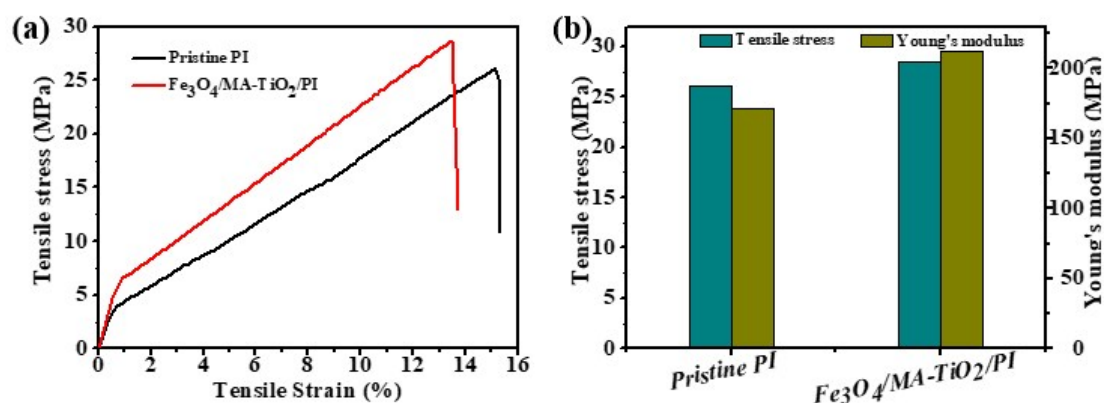


Figure S3 (a) Tensile stress-strain curves and Young's modulus (b) of pristine PI and as-prepared Fe₃O₄/MA-TiO₂/PI membranes.

The tensile test was also employed to quantitatively analyse the mechanical flexibility of the as-prepared membranes. One can clearly see from Fig. S3b that the Young's modulus and tensile stress of pristine PI are 171.8 and 26.1MPa, respectively, while the Young's modulus of the Fe₃O₄/MA-TiO₂/PI membrane is around 212.1 and tensile stress around 28.6 MPa. The slightly increased tensile stress behavior of Fe₃O₄/MA-TiO₂/PI membrane may be ascribed to the affinity among nanoparticles, MA-TiO₂ sol and nanofibers. Significantly, it was worth mentioning that the as-prepared membrane combines the excellent mechanical properties of the PI membrane, the pH-responsive wettability and the magnetic properties of the Fe₃O₄ nanoparticles. Therefore, the Fe₃O₄/MA-TiO₂/PI membrane possessed good mechanical flexibility, which can be used as a promising material in the application of oil/water separation.

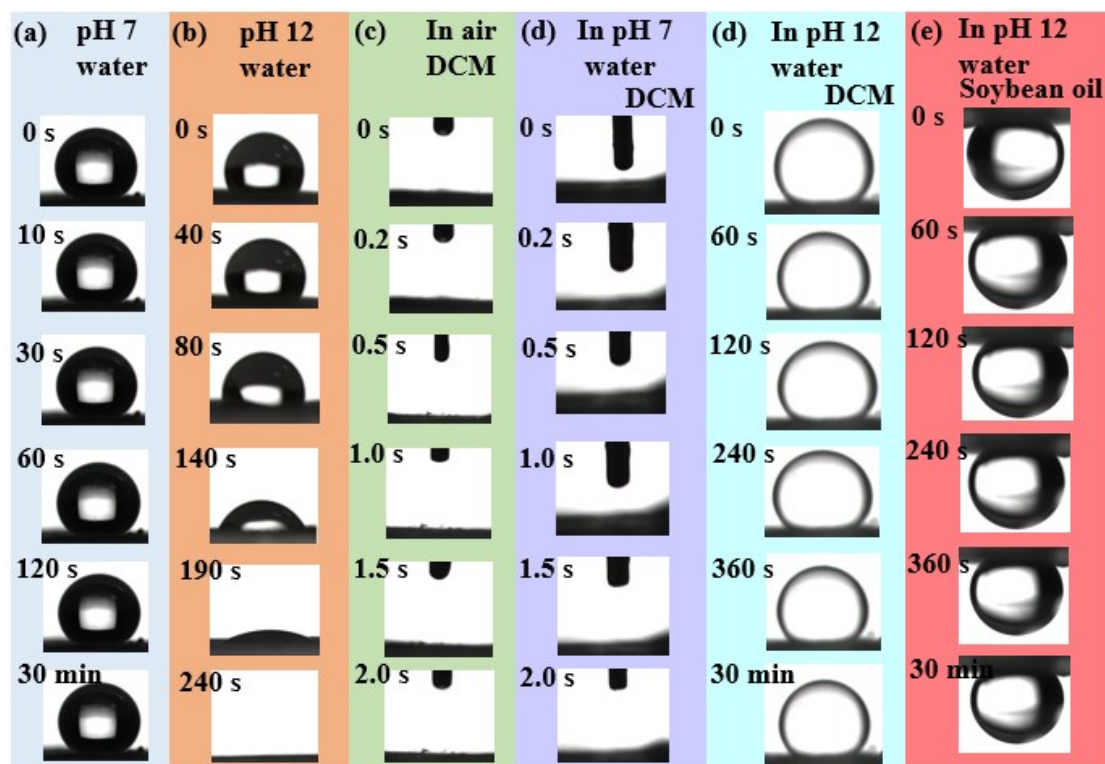


Figure S4 Time dependence of water and oil contact angle of the as-prepared membrane

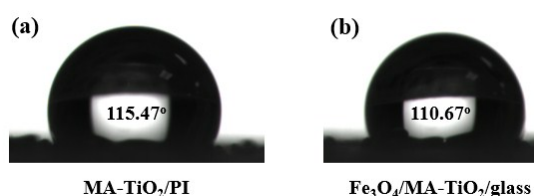


Figure S5 Contact angle images of water droplet on (a) MA-TiO₂/PI membrane and (b) Fe₃O₄/MA-TiO₂/glass slide

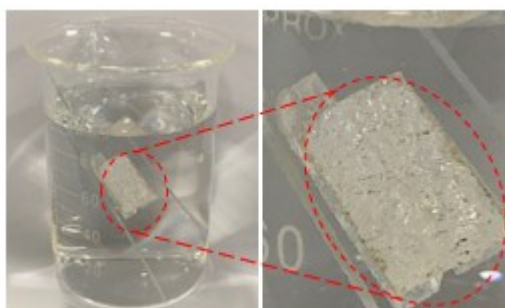


Figure S6 Mirror-like phenomenon of the Fe₃O₄/MA-TiO₂/PI membrane

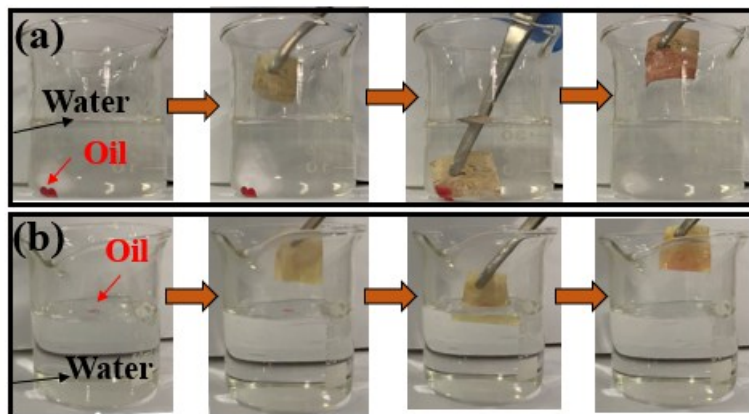


Figure S7 Photographs showing the absorption of dyed dichloromethane (a) and paraffin (b) from water by $\text{Fe}_3\text{O}_4/\text{MA-TiO}_2/\text{PI}$ membrane.

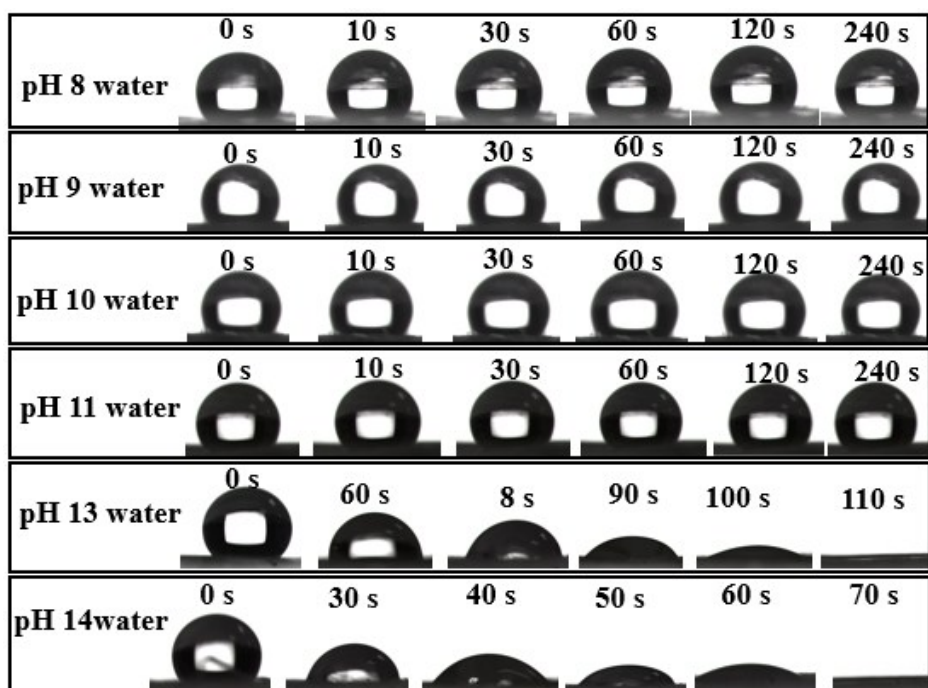


Figure S8 Contact angle images of water droplet with different pH on the as-fabricated $\text{Fe}_3\text{O}_4/\text{MA-TiO}_2/\text{PI}$ membrane

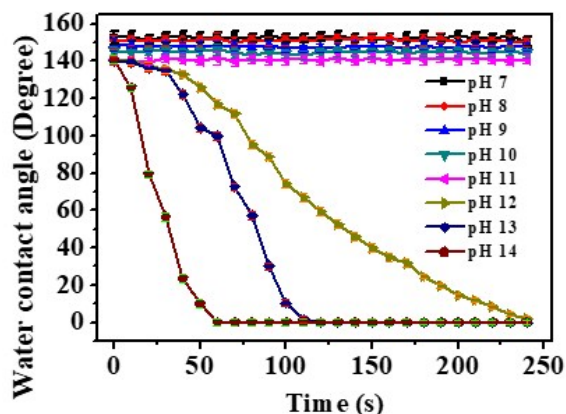


Figure S9 Dynamic contact angle for water drops of different pH values on the $\text{Fe}_3\text{O}_4/\text{MA-TiO}_2/\text{PI}$ membrane

As Fig. S8 and Fig. S9 shows, when water droplets having a pH value of 8-10 loaded on the membrane, the membrane surfaces remained superhydrophobicity with WCAs over 150° for more than 4 minutes. Whereas, with the increasing pH value, the WCA decreased dramatically, from rather hydrophobic 152.65° to quite hydrophilic 0° and the water droplet even permeate completely through the membrane. These results demonstrate that the $\text{Fe}_3\text{O}_4/\text{MA-TiO}_2/\text{PI}$ membrane possesses excellent superhydrophobicity in neutral environments, and is able to switch from superhydrophobicity to superhydrophilicity in a strong basic environment.

The corresponding wettability transformation mechanism of the smart membrane is explained as follows. In the preparation of $\text{Fe}_3\text{O}_4/\text{MA-TiO}_2$ coating solution, coordination chemistry of MA-TiO₂ happened, thus the formation of the $\equiv\text{Ti-O-Ti-OOC-}$. Carboxyl groups are mostly in the protonated state when in contact with a neutral water droplet and the exterior of the as-prepared membrane was dominated by hydrophobic alkyl chain of MA molecules. As a result, the membrane exhibits hydrophobic property. In addition, the hierarchical micro/nanostructures on the surface further enhanced the hydrophobicity. On the contrary, when contacting with alkaline water, the titanium-carboxylate coordination bond broke and the ionic MA disappeared [7-9]. The desorption of the MA molecules from the solid surface will not

only increase solid-surface free energy but also simultaneously reduce water surface tension locally, thus leading to a hydrophilic surface. In this condition, the water phase will invade the rough micro/ nanostructure of the surface. Obviously, the aforementioned results were in good agreement with the theory explanation, revealing that the intelligent membrane has been prepared successfully.

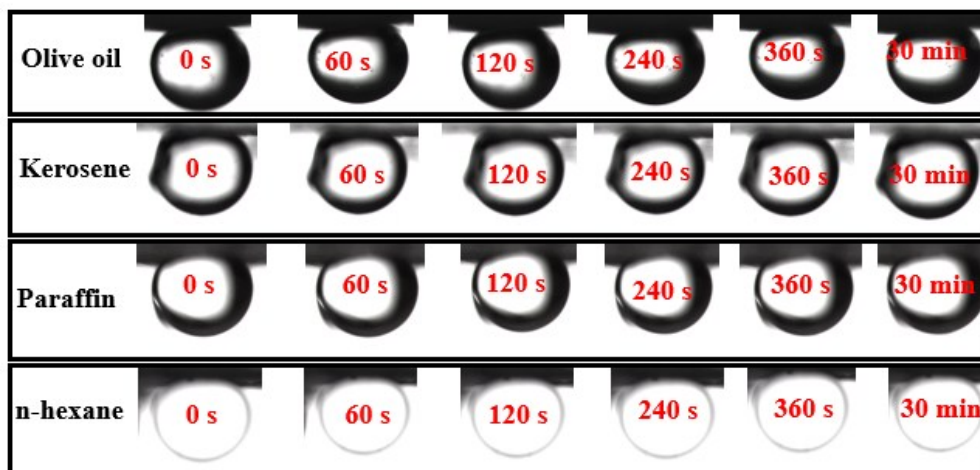


Figure S10 Time dependence of oil contact angle of the as-prepared $\text{Fe}_3\text{O}_4/\text{MA-TiO}_2/\text{PI}$ membrane

Young's state	Wenzel's state	Cassie's state	Intermediate state
(a)	(b)	(c)	(d)
$\gamma_{lv} \cos \theta = \gamma_{sv} - \gamma_{sl}$	$\cos \theta^* = R_f \cos \theta$	$\cos \theta^* = f_1 \cos \theta_1 + f_2 \cos \theta_2$	$\cos \theta^* = f(R_f \cos \theta + 1) -$

Figure S11 Schematic diagrams of a water droplet on (a) a flat surface and rough surfaces in (b) Wenzel, (c) Cassie, and (d) Intermediate wetting states in air

Underwater Young's	Underwater Wenzel's	Underwater Cassie's state	Underwater Intermediate
--------------------	---------------------	---------------------------	-------------------------

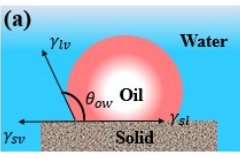
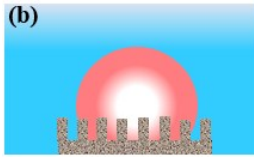
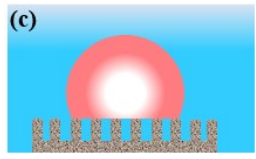
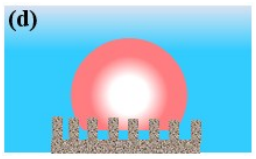
state	state		state
			
$\gamma_{lv} \cos \theta_{ow} = \gamma_{sv} - \gamma_{sl}$	$\cos \theta_{ow}^* = R_f \cos \theta_{ow}$	$\cos \theta^* = f_1 \cos \theta_{ow1} + f_2 \cos \theta_{ow2}$	$\cos \theta_{ow}^* = f(R_f \cos \theta_{ow} + 1)$

Figure S12 Schematic diagrams of underwater oil droplets on (a) a flat surface, and (b) Wenzel, (c) Cassie, and (d) Intermediate wetting states rough surfaces

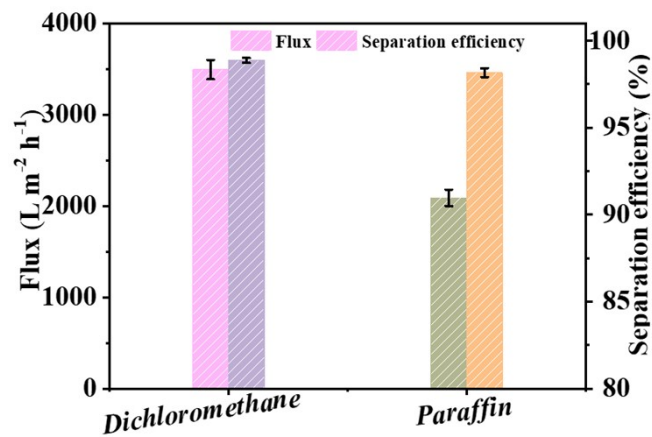


Figure S13 Separation performance of the MA-TiO₂/PI membrane towards dichloromethane (heavy oil)/water and paraffin (light oil)/water mixtures.

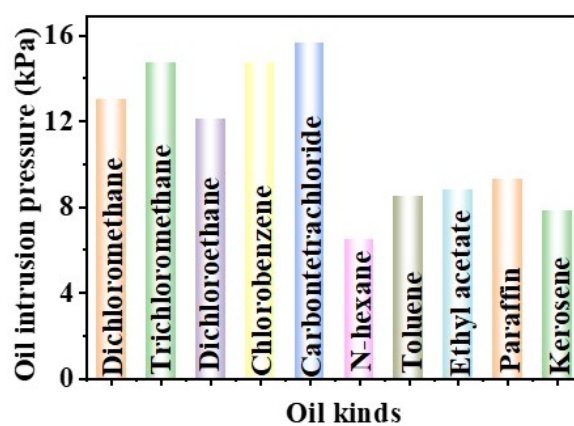


Figure S14 Intrusion pressures for different oils

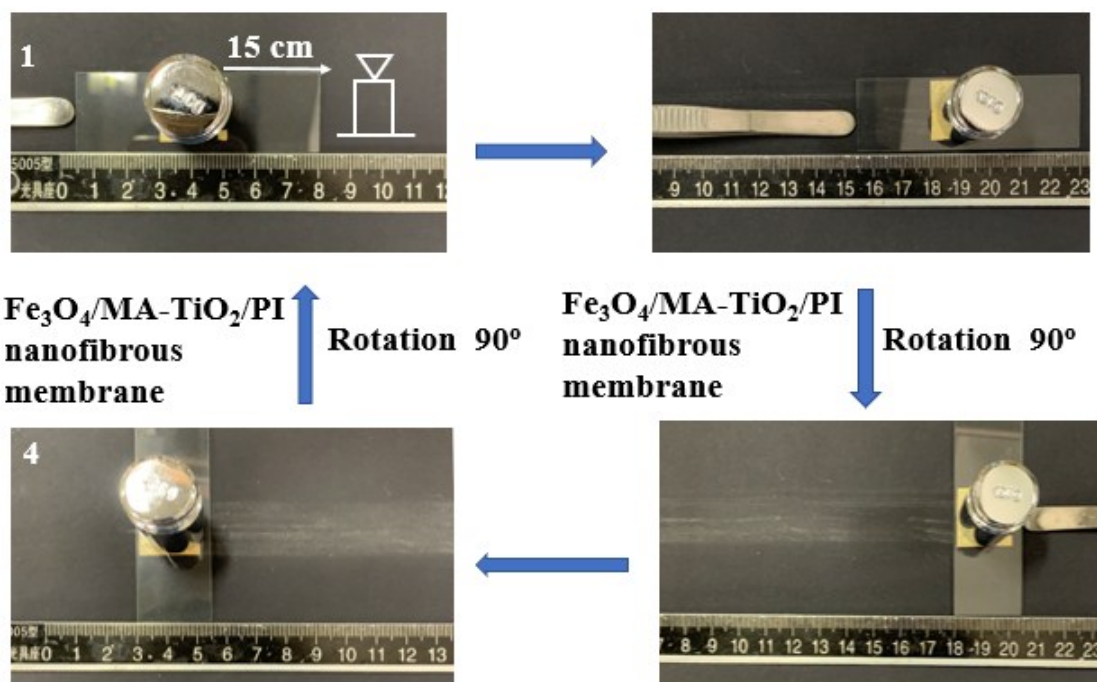


Figure S15 Photographs of one cycle of the sandpaper abrasion test, from the top view

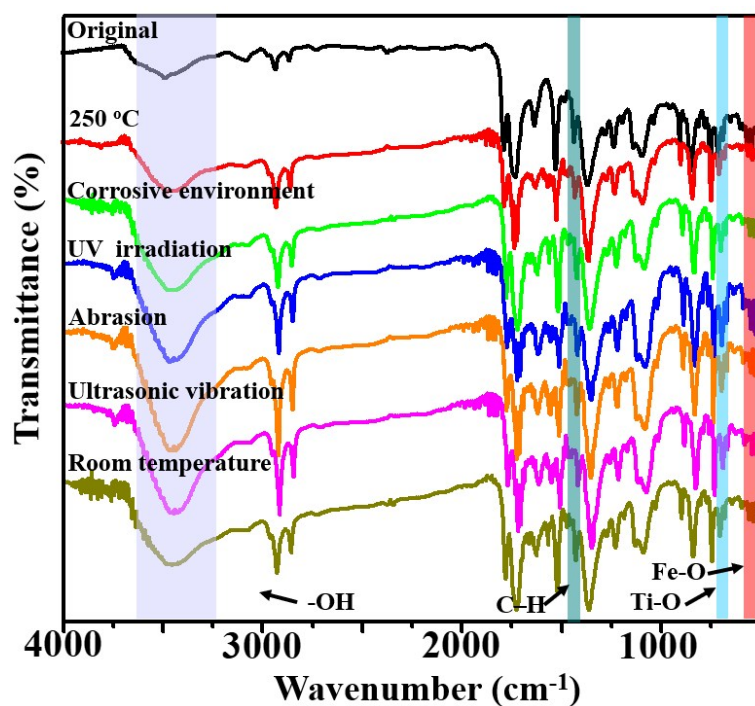


Figure S16 FTIR spectrum of the $\text{Fe}_3\text{O}_4/\text{MA-TiO}_2/\text{PI}$ membrane after durability test

[1] W. Ma, Q. Zhang, S.K. Samal, F. Wang, B. Gao, H. Pan, H. Xu, J. Yao, X. Zhan, S.C.D. Smedt, Core-sheath structured electrospun nanofibrous membranes for oil-water separation, *Rsc Advances*, 6 (2016) 41861-41870.

- [2] J.L. Gong, B. Wang, G.M. Zeng, C.P. Yang, C.G. Niu, Q.Y. Niu, W.J. Zhou, L. Yi, Removal of cationic dyes from aqueous solution using magnetic multi-wall carbon nanotube nanocomposite as adsorbent, *Journal of Hazardous Materials*, 164 (2009) 1517-1522.
- [3] E. Ranjbakhsh, A.K. Bordbar, M. Abbasi, A.R. Khosropour, E. Shams, Enhancement of stability and catalytic activity of immobilized lipase on silica-coated modified magnetite nanoparticles, *Chemical Engineering Journal*, 179 (2012) 272-276.
- [4] W. Shen, L. Feng, H. Feng, A. Lei, Divalent silver oxide-diatomite hybrids: Synthesis, characterization and antibacterial activity, *Ceramics International*, 39 (2013) 5013-5024.
- [5] S. Yu, J. Wan, K. Chen, A facile synthesis of superparamagnetic Fe₃O₄ supraparticles@MIL-100(Fe) core-shell nanostructures: Preparation, characterization and biocompatibility, *Journal of Colloid and Interface Science*.
- [6] S.Y. Mak, D.H. Chen, Binding and Sulfonation of Poly(acrylic acid) on Iron Oxide Nanoparticles: a Novel, Magnetic, Strong Acid Cation Nano-Adsorbent, *Macromolecular Rapid Communications*, 26 (2010) 1567-1571.
- [7] X. Zhiguang, Z. Yan, W. Hongxia, W. Xungai, L. Tong, A superamphiphobic coating with an ammonia-triggered transition to superhydrophilic and superoleophobic for oil-water separation, *Angew Chem Int Ed Engl*, 127 (2015) 4610-4613.
- [8] S. Liu, G. Han, M. Shu, L. Han, S. Che, Monodispersed inorganic/organic hybrid spherical colloids: Versatile synthesis and their gas-triggered reversibly switchable wettability, *Journal of Materials Chemistry*, 20 (2010) 10001-10009.
- [9] Z. Xu, Z. Yan, L. Dai, L. Tong, Multi-Responsive Janus Liquid Marbles: The Effect of Temperature and Acidic/Basic Vapors, *Particle & Particle Systems Characterization*, 31 (2014) 839-842.